Available online at www.sciencedirect.com
SCIENCE DIRECT®
Optics Communications 264 (2006) 426–434
OPTICS COMMUNICATIONS
www.elsevier.com/locate/optcom

Adiabatic passage schemes in coupled semiconductor nanostructures

Ulrich Hohenester [a,*], Jaroslav Fabian [b], Filippo Troiani [c]

[a] Institut für Physik, Karl-Franzens-Universität Graz, Universitätsplatz 5, 8010 Graz, Austria
[b] Institut für Theoretische Physik, Universität Regensburg, 93040 Regensburg, Germany
[c] Departamento de Fisica Teorica, Universidad Autonoma de Madrid, 28049 Madrid, Spain

Received 27 October 2005; accepted 26 January 2006

Abstract

Adiabatic passage schemes in coupled semiconductor quantum dots are discussed. For optical control, a doped double-dot molecule is proposed as a qubit realization. The quantum information is encoded in the carrier spin, and the flexibility of the molecular structure allows to map the spin degrees of freedom onto the orbital ones and vice versa, which opens the possibility for high-finesse quantum gates by means of stimulated Raman adiabatic passage. For tunnel-coupled dots, adiabatic passage of two correlated electrons in three coupled quantum dots is shown to provide a robust and controlled way of distilling, transporting and detecting spin entanglement, as well as of measuring the rate of spin disentanglement. Employing tunable interdot coupling the scheme creates, from an unentangled two-electron state, a superposition of spatially separated singlet and triplet states, which can be discriminated through a single measurement. Finally, we discuss phonon-assisted dephasing in quantum dots, and present control strategies to suppress such genuine solid-state decoherence losses.

PACS: 73.21.La; 71.35.−y; 03.67.Mn; 02.60.Pn

Keywords: Quantum dots; Adiabatic passage; STIRAP; Quantum control

1. Introduction

The emerging field of quantum information has initiated a tremendous quest for control strategies of quantum matter [1]. Here, the objective is to manipulate the state of a single quantum system with highest possible precision, or to let two quantum systems interact in a well-controlled fashion. For systems isolated from their environment a remarkable theorem states that under broad conditions such quantum control is either possible with a fidelity of precisely one, or not at all [2]. No corresponding conclusions generally prevail for systems in contact with their environment. A striking exception is the celebrated *stimulated Raman adiabatic passage* (STIRAP) scheme [3,4] that allows for an ideal population transfer between two long-lived quantum states, optically connected to a third auxiliary state, despite possible environment losses of the interconnecting state. This is achieved by driving the system with two strong laser fields into a state which is completely stable against absorption and emission from the radiation fields, and by adiabatically channeling the population between the two long-lived states, through slow variation of the laser intensities, without ever populating the leaky auxiliary state. As a further advantage, such control does not require a detailed knowledge of the system parameters and therefore is of very robust nature.

Although STIRAP control was originally designed for atomic systems [3,4], its ability to suppress environment losses and its robustness render this scheme ideal for quantum control in the solid state. In particular for semiconductor quantum dots [7–10], or *artificial atoms*, as

* Corresponding author. Tel.: +43 316 3805227; fax: +43 316 3809820.
E-mail address: ulrich.hohenester@uni-graz.at (U. Hohenester).

0030-4018/$ - see front matter © 2006 Elsevier B.V. All rights reserved.
doi:10.1016/j.optcom.2006.01.064

they are often called because of their atomic-like density of states, a variety of quantum-information and quantum-optics applications have been envisioned [11,12]. Semiconductor quantum dots are small islands of semiconducting material, typically consisting of millions of atoms, embedded in a surrounding host material, where carrier confinement within these islands is achieved by use of different semiconductor materials or by applying external gate voltages. These structures exhibit a number of striking features, such as, e.g., ultralong relaxation and decoherence times or a strong enhancement of Coulomb correlation effects. The combination of these two effects has allowed the demonstration of fundamental quantum coherence effects in this class of material, including coherent carrier [13] and entanglement control [14,15], and Rabi flopping [16–18]. Hitherto the huge experimental progress in this field of research is mostly due to major advancements in sample preparation, whereas from a quantum-control perspective there is still plenty of room at the bottom.

This paper is devoted to a discussion of possible adiabatic-passage schemes in semiconductor quantum dots that would outperform existing control strategies – an issue of great importance for the ambitious quantum information implementations presently under consideration. In Section 2 we review some of our older proposals of optical STIRAP control in coupled semiconductor quantum dots [19,6]. We show how charged-exciton states can be exploited for population transfer of carries, and how unconditional and conditional quantum gates can be implemented by means of adiabatic control. In Section 3 we discuss adiabatic population transfer in tunnel-coupled dots that are populated by two electrons. Because of strong Coulomb correlation effects the carrier states become substantially renormalized, which can be used for entanglement detection, transport, as well as disentanglement measurement, all in a robust way, without the need for fine tuning or precise knowledge of spectral or pulse parameters [20]. Section 4 addresses the issue of phonon-assisted dephasing, a decoherence channel that can even affect the long-lived ground states of semiconductor nanostructures. We show that appropriate pulse shaping allows to suppress such genuine solid-state decoherence losses.

2. STIRAP in semiconductor nanostructures

A typical STIRAP level scheme is shown in Fig. 1a [3,4], consisting of two long-lived states 0 and 1 which are connected through a third short-lived state 2. In Ref. [19] we showed that such a scheme corresponds to the situation where a coupled quantum-dot molecule is populated by one surplus hole, as depicted in Fig. 2. Vertically coupled quantum dots naturally occur in self-organized growth, where the alignment of the dots on top of each other is mediated by strain [7,21]. The two truncated cones in the figure correspond to the islands of low-band-gap material, within which the carriers become confined, and the dot at the bottom is assumed to be larger than the dot at the top – a configuration in close resemblance to actual dot samples. For this dot confinement the solutions of the three-dimensional Schrödinger equation are depicted in the different panels of Fig. 2 (we use material parameters representative for GaAs-based materials [19,22,23] and assume low temperatures throughout). Because of the larger mass of holes in semiconductors, the hole wavefunction becomes localized in either the lower (panel a) or upper (panel b) dot. These two states are correspondingly associated to the long-lived states 0 and 1 of the STIRAP scheme, where hole charging is achieved by placing the dot molecule in a field-effect structure. Excited electron and hole states are typically a few tens of meV higher in energy and can thus be safely neglected [7,8]. Phonon scattering between the two hole states, which is expected to be the

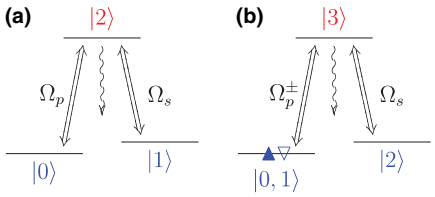

Fig. 1. Prototypical level schemes for the implementation of STIRAP. (a) Λ-type level scheme with two long-lived states 0 and 1, and a short-lived interconnecting state 2. Ω_p and Ω_s denote the pump and Stokes pulse, respectively, that couple the 0–2 and 1–2 transitions [3,4]. (b) Extended scheme that allows the implementation of quantum gates [5,6], with the spin-degenerate ground states 0 and 1, the long-lived state 2, and the interconnecting state 3. The 0–3 and 1–3 transitions can be addressed by different light polarizations $\Omega_p^{\pm}$. For discussion, see text.

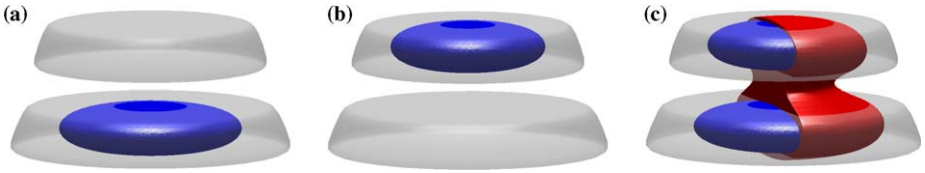

Fig. 2. Schematic illustration of the proposed double-dot structure and the carrier wavefunctions. The confinement potential consists of two truncated-cone-shaped regions of low-band-gap material. The upper cone has diameters of 14 and 16 nm, and a height of 3 nm, whereas the diameters of the lower cone have been enlarged by 20%. The distance between the two dot centers is 5 nm. Panels (a) and (b) show, respectively, the square modulus of the hole ground and first excited wavefunction, which is either localized in the lower or upper dot. Panel (c) shows the charged exciton state (isosurface at 25% of the maximum value), where the electron wavefunction (red, cut off for clarity) extends over the whole structure because of the lighter electron mass, and allows optical coupling to both hole states [19].

major source of decoherence, can be strongly suppressed in this system by properly choosing the dot sizes and the dot distance [24]. The interconnecting auxiliary state is given by the charged-exciton state, Fig. 2c, which consists of two holes and one electron. Here, the electron is delocalized over the whole structure, because of the lighter electron mass in GaAs-based structures, which allows optical coupling to both hole states 0 and 1. Within this scheme it is possible to transfer the hole between the two dots in the usual STIRAP scheme, i.e. by use of the counter-intuitive order where the Stokes pulse precedes the pump pulse. For the quantum dots under study (i.e. strong confinement regime) typical pulse durations are of the order of tens of picoseconds, in accordance to recent experiments demonstrating Rabi flopping in quantum dots [18,8].

The above scheme allows for a proof-of-principle experiment of STIRAP in semiconductor quantum dots. It was elaborated by Pazy et al. [25] for a readout scheme of quantum registers, and by Kis and Paspalakis [26] for the controlled creation of entangled exciton states. In Ref. [6] we extended, following earlier work that showed how STIRAP-related schemes can be used for entanglement creation [27] and qubit rotations [5], our original proposal to allow for quantum computation in an array of coupled quantum dots. Our approach, which we shall briefly summarize now, rests on the modified level scheme depicted in Fig. 1b, originally proposed by Kis and Renzoni [5], in which the quantum information is encoded in the long-lived states 0 and 1. The long-lived state 2 and the short-lived state 3, to which all other states are optically connected, are then used as auxiliary states during the quantum gates. In fact, all these states can be naturally identified within our double-dot molecule. For conceptual clarity, in the following we keep the picture of a hole-doped structure, although our proposal works equally well for an electron-doped molecule, which might be beneficial for the suppression of decoherence [6]. The central observation of our proposal concerns the fact that carriers in semiconductors possess both charge and spin degrees of freedom, where spin is considered as a highly promising candidate for quantum memory because of its long life and coherence times [28], and that STIRAP allows to map the spin degrees of freedom onto the orbital ones and vice versa. We associate the states 0 and 1 to the two different spin orientations of the hole localized in the larger dot, Fig. 2a, and assume that the 0–3 and 1–3 transitions can be discriminated by use of the usual optical selection rules [28] (as indicated by the two different pump fields $\Omega_{\mathrm{p}}^{\pm}$).

Within this level scheme of Fig. 1b it becomes possible to perform generic unconditional quantum gates along the lines discussed in Ref. [5], i.e., by applying two STIRAP pulse sequences in series. On the other hand, the mapping between spin and orbital degrees of freedom can be also utilized for conditional gates. Consider a qubit in state $\alpha|0\rangle + \beta|1\rangle$, where the quantum information is fully encoded in the spin degrees of freedom. By applying one STIRAP sequence, we next transform the state to $\alpha|0\rangle + \beta|2\rangle$ where the quantum information is mapped onto the orbital degrees of freedom. By inspection of the hole wavefunctions depicted in panels (a) and (b) of Fig. 2, we observe that a neighbor quantum dot molecule will see a different charge distribution, depending on whether the system is in state 0 or 2 (i.e., the surplus carrier in either the lower or upper dot), which is accompanied by different Coulomb forces exerted on the neighbor (target) molecule. The resulting shift of transition frequencies can be used to perform a conditional gate (similar to the unconditional gate discussed above) at the shifted frequencies. After the manipulation of the quantum information in the target qubit, the quantum information of the first (control) qubit is rotated back to the spin degrees of freedom by use of a further STIRAP pulse sequence. This scheme, which is described in more detail in Ref. [6], clearly highlights the flexibility of wavefunction engineering in the solid state. Other work proposed similar schemes based on the quantum-confined Stark effect [29] or Förster-type processes [30]. Addressing of individual molecules, whose transition frequencies differ because of dot size fluctuations, can be achieved in small quantum dot arrays through spectral filtering, while for larger dot arrays an additional nanofocusing of light, such as envisioned in Ref. [31], might be requested. The pertinent life and coherence times for spin excitations in quantum dots are of the order of tens of nanoseconds [32,33], where hyperfine interactions with nuclear spins are expected to be the major source of decoherence (see Refs. [34,15] for a discussion and for possible control protocols).

Quantum gates do not exhaust the possible use of STIRAP in semiconductor nanostructures for quantum-information processing. In fact, adiabatic passages within similar level schemes can also be exploited to optimize single-photon sources. There, the dot is embedded in a three-dimensional microcavity which creates the conditions for the contextual achievement of high collection efficiencies and photon indistinguishabilities: while the former feature is strongly enhanced thanks to the highly directional emission from the cavity, the latter calls for the emitter state to be coherently driven from the initial to the radiating level. Quite generally, the issue here is no longer that of avoiding the population of the leaky state, as in the case of the spin manipulation; one rather needs the radiative relaxation to occur through a different channel than the one the dot is excited through. The conceptually straightforward form of differentiating the emitted radiation from the incoming one is the inclusion of a non-radiative energy relaxation between the system's excitation and de-excitation. While a suitable engineering of the dot and cavity parameters can result in a sensible increasing of the photon indistinguishabilities sofar achieved [35,36], the use of STIRAP (together with the achievement of a strong-coupling regime) allows, in principle, to approach the optimal device performance [37], with the cavity mode playing the role of the Stokes laser. It is finally worth mentioning that single-photon sources are the fundamental building block within

different kinds of quantum devices. In fact, they are directly required for linear-optics quantum computation; besides, couples of indistinguishable photons can be manipulated into entangled photon pairs, which are essential for implementing quantum teleportation.

3. Entanglement distillation by adiabatic passage

Contrary to the previous section, where we studied optical control of self-assembled quantum dots, in the following we consider voltage control of gate-induced quantum dots, where electrons in a narrow quantum well become confined by means of external gate voltages [9,10]. A particular implementation of quantum information processing in such nanostructures relies on electron spins in coupled quantum dots, proposed as qubits for quantum inverters [38] and for universal gating in quantum computation [39]. Impressive progress has recently been made for coherent control of electronic states [10,40,41], spin coherence [42], and spin entanglement [15]. The creation and detection of entanglement in a controlled and robust way is a major task. It has been proposed that entangled two-electron spin states can be produced by tuned quantum gates [39,43,44], by filtering through time-dependent barriers [50], or by projective measurements [45,46]. Entanglement is proposed to be detected by current noise measurements [49,47]. In this section we introduce an alternative scheme based on adiabatic passage, which provides a robust and controlled way of distilling, transporting and detecting spin entanglement, as well as of measuring the rate of spin disentanglement. We call the scheme, which can be realized by current experimental techniques, entanglement distillation by adiabatic passage (EDAP) [20]. Although EDAP is general enough to be applicable to a general three level quantum mechanical system with two electrons, such as atoms in optical lattices or molecules [48], we will present it using the physics of an array of three coupled quantum dots.

Consider two electrons in three laterally confined quantum dots, labeled 1–3. The dots 1 and 2, as well as 2 and 3 are coupled via electrostatic gates. The corresponding tunneling amplitudes, t_{12} and t_{23}, can be tuned on sub-nanosecond time scales by modulating the gate voltages. Let the two electrons reside initially on dots 1 and 2, as shown in Fig. 3. The spin state of the system can be, quite generally, written as a superposition of the singlet state $|S\rangle_{12}$, describing electrons located on dots 1 and 2, as well as the triplet states $|T_{S_z}\rangle_{12}$ of the spin projection S_z (-1, 0, or 1), extended over dots 1 and 2,

$$\Psi(0) = a|S\rangle_{12} + b|T_0\rangle_{12} + c|T_1\rangle_{12} + d|T_{-1}\rangle_{12}. \quad (1)$$

The EDAP scheme is based on our finding of a strong correlation between adiabatic passage and entanglement: a single adiabatic pulse sequence induces entirely different adiabatic passages of different Bell (maximally entangled) spin states. More specifically, the EDAP pulse sequence, to be discussed below, brings this initial two-electron spin state into a superposition of spatially separated entangled states

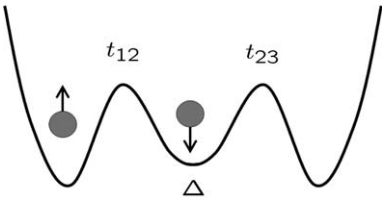

Fig. 3. Two electrons with opposite spins in an array of three coupled dots. The tunneling amplitudes between the dots are denoted as t_{12} and t_{23}. The energy offset of the middle dot is Δ. By manipulating the gates t_{12} and t_{23} an initial spin uncorrelated state becomes a superposition of two entangled states, the singlet with the electrons on dots 1 and 2, and a triplet, with electrons on dots 2 and 3. The detection of charge on dot 1 collapses the superposition to the singlet, the detection of an absence of charge on the same dot collapses the state to a triplet.

$$\Psi(\infty) = a'|S\rangle_{12} + b'|T_0\rangle_{23} + c'|T_1\rangle_{23} + d'|T_{-1}\rangle_{23}. \quad (2)$$

The primed coefficients have the same amplitudes as the unprimed ones. The singlet remains on dots 1 and 2, while the triplet states are now shifted by one dot (they extend over dots 2 and 3). Detection of charge on dot 1 distills the singlet. If no charge is detected on the dot, a triplet is distilled. The scheme cannot discriminate among the different triplet states without an additional local magnetic field control.

Our system can be well described by the time-dependent Hubbard Hamiltonian [20]

$$H = \sum_{i\lambda} \varepsilon_i n_{i\lambda} + \sum_i U n_{i\uparrow} n_{i\downarrow} + \sum_{ij,\lambda} t_{ij} a^+_{i\lambda} a_{j\lambda}, \quad (3)$$

with the Fermi creation ($a^+_{i\lambda}$) and annihilation ($a_{i\lambda}$) operators for dot i (1–3) and spin $\lambda = \uparrow, \downarrow$, and number operators $n_{i\lambda} = a^+_{i\lambda} a_{i\lambda}$. The confining energies ε_i do not depend on spin. We take $\varepsilon_1 = \varepsilon_3 = 0$, while setting an offset for the middle dot $\varepsilon_2 = \Delta$. The offset can be controlled electrostatically, or it can be fixed within a useful spectral range as discussed below. Only on-site Coulomb U interaction is included in our model, while off-site interactions do not qualitatively change our conclusions [20]. Tunneling amplitudes representing interdot couplings are t_{ij}. Here only t_{12} and t_{23} are not zero and depend on time t, so that $H = H(t)$. The interdot couplings are modulated by electrostatic gates defining interdot barriers. In the examples below we use generic values of $U = 1$ meV and maximum tunneling amplitudes smaller than 0.1 meV. We will see that Δ needs to be of order U for EDAP to work well.

The time dependent spectrum of H, in the presence of interdot coupling pulses, is shown in Fig. 4a. We take Gaussian pulses of the form $t_{ij}(t) = t_0 \exp(-t^2/2\tau^2)$, where t_0 is the maximum pulse strength and τ is the dispersion. The overlap between the pulses is taken to be 2τ, the width of one pulse. For the case of EDAP the pulse sequence in which t_{12} precedes t_{23} is counterintuitive (for reasons to be given below), while the opposite sequence is intuitive. Adiabatic passage of single electrons in three coupled quantum dots has been proposed in Ref. [51].

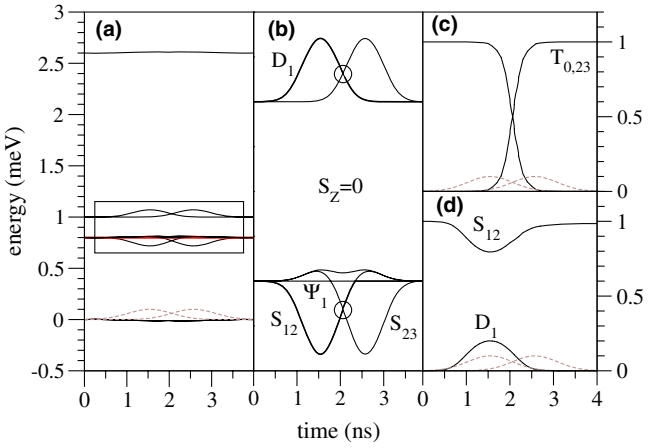

Fig. 4. Time evolution of the energy spectrum and the population probabilities. (a) The spectrum of Hamiltonian (3) with time dependent pulses t_{12} and t_{23} indicated by dashed lines (the order of the pulses is not important here). (b) Zoom of the spectral evolution of the singlet and double occupancy states with $S_z = 0$. The horizontal line is the trapped level corresponding to Ψ_1. The circles indicate that there is a weak level anticrossing where the passage is rapid. (c) Time evolution of the population of triplets $|T_0\rangle_{12}$ and $|T_0\rangle_{23}$. (d) Time evolution of the population of singlet $|S\rangle_{12}$ and double occupancy state D_1 as obtained from full many-body calculations. Taken from Ref. [20].

There are three weakly coupled groups of states shown in Fig. 4. The lowest states with energy $E \approx 0$ consist of electrons occupying mainly dots 1 and 3. The highest state with energy $E \approx U + 2\Delta$ is for a double occupancy of dot 2. The states relevant for EDAP have $E \approx U$, Δ, and comprise electron singlets and triplets on neighboring dots. These states are magnified in Fig. 4b. As discussed in Appendix A, the eigenstates of the Hubbard Hamiltonian can be obtained within the respective subspaces of singlet and triplet states. Most importantly, we obtain the four trapped states [20]

$$\begin{aligned}
\Psi_1 &= \sin\varphi|T_0\rangle_{12} - \cos\varphi|T_0\rangle_{23},\\
\Psi_2 &= \sin\varphi|T_1\rangle_{12} - \cos\varphi|T_1\rangle_{23},\\
\Psi_3 &= \sin\varphi|T_{-1}\rangle_{12} - \cos\varphi|T_{-1}\rangle_{23},\\
\Psi_4 &= (|D\rangle_1 - |D\rangle_2 + |D\rangle_3)/\sqrt{3},
\end{aligned} \tag{4}$$

whose energies do not depend on the tunneling amplitudes, where $\varphi = \varphi(t)$ is given by $\tan\varphi = t_{12}/t_{23}$. The absence of singlet states in these states is striking. States Ψ_1 through Ψ_3, which comprise triplets only, can be used for a STIRAP scheme with the counterintuitive pulse sequence (t_{12} precedes t_{23}), to move triplets on dots 1 and 2 to dots 2 and 3. Such a transfer, calculated numerically using $H(t)$ from Eq. (3), is shown in Fig. 4c. State Ψ_4, which is trapped only if $\Delta = 0$, does not depend on the tunneling amplitudes and thus cannot be used for a passage. We call the state globally trapped.

The reason why triplet states can be transferred by passage is the fact that they do not couple to doubly occupied states D. On the other hand, singlet states do couple to D's; as a result their dynamics is more complicated. Our goal is to prevent $|S\rangle_{12}$ from transfer. The way to do this is to introduce the energy offset Δ on the order of U. In this case a two level system of $|S\rangle_{12}$ and D_1 rather faithfully describes the dynamics of these two states. During an adiabatic pulse the singlet $|S\rangle_{12}$ evolves to itself, while the doublet is briefly populated in the process, as shown by numerical simulation in Fig. 4d. For this to work it is crucial that the resonance condition $\Delta = U$ is avoided. At resonance the evolution is a Rabi oscillation whose outcome depends on the pulse areas – the scheme would not be robust (see Fig. 5). In fact, the adiabatic passage of the singlet requires also a rapid passage at anticrossings indicated in Fig. 4b. Fortunately, the conditions for the rapid passage are rather favorable and do not limit the adiabatic passage itself [20]. Since we require that $\Delta \neq 0$ for the entanglement separation (the case $\Delta = 0$ could still be used for triplet state transfer), it is not important to use counterintuitive sequencing. Intuitive sequence (t_{23} precedes t_{12}), in which the passage is not done through the trapped state, works equally well.

To identify numerically the regime of applicability of the scheme, we define EDAP efficiency w as

$$w = |\langle\Psi(\infty)|S\rangle_{12}|^2 + |\langle\Psi(\infty)|T_0\rangle_{23}|^2 \tag{5}$$

for a state $\Psi(t)$ with the initial condition $\Psi(0) = a^+_{1\uparrow}a^+_{2\downarrow}|0\rangle$. The efficiency for the intuitive sequence is shown in the left

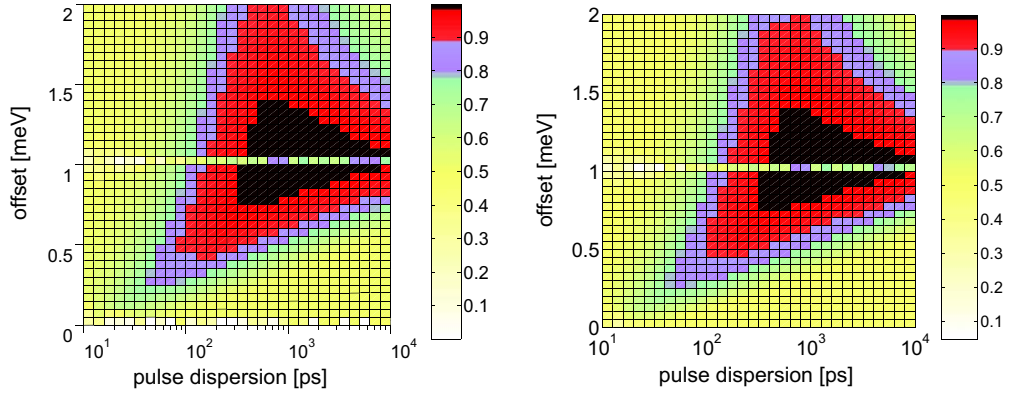

Fig. 5. EDAP efficiency with intuitive (left panel) and counter-intuitive (right panel, see also Ref. [20]) pulse sequence as a function of offset Δ and pulse time τ. The structures at $\Delta \approx U = 1$ meV and at $\Delta = 0$ are caused by resonant conditions – the passage is not robust here as it depends on the pulse area.

panel of Fig. 5, while that of the counterintuitive sequence in the right panel. Both figures show the efficiency for a large range of pulse times and energy offsets. It is evident that both schemes work very well (with efficiencies close to 100%) for a large enough window of parameters to be relevant in realistic systems as well. Demonstrating the robustness of the scheme of our ideal model is of great importance since the presence of decoherence or higher-level triplet states will certainly lower the efficiency and reduce the useful parameter range.

Finally, we address the question of possible asymmetry in energies ε_1 and ε_3. The adiabatic passage of the singlet channel requires that $\delta\varepsilon \equiv |\varepsilon_3 - \varepsilon_1| \leqslant \Delta$. The triplet channel is more restrictive, since the condition is $\delta\varepsilon \leqslant t_0^2/U$, that is, the level asymmetry should be below the exchange energy. Experimentally this is not a problem as individual dots' energies can be controlled electrically. However, it turns out that EDAP still works as a distillation scheme even if $\delta\varepsilon \geqslant t_0^2/U$ (restricted only by $\delta\varepsilon \leqslant \Delta$). In this regime $|T_{12}\rangle$ evolves to $|T_{23}\rangle + \alpha|T_{12}\rangle$ instead of to just $|T_{23}\rangle$. The singlet channel is still very robust: $|S_{12}\rangle$ goes to $|S_{12}\rangle$. This means that starting from an uncorrelated state EDAP will uniquely result in triplet $|T_{23}\rangle$ if a charge on dot 3 is detected, and to $|S_{12}\rangle + \alpha|T_{12}\rangle$ if charge on 1 is observed. The singlet $|S_{12}\rangle$ can be distilled (purified) from this mixture by successive applications of EDAP, as the proportion of $|T_{12}\rangle$ will diminish as $\sim\alpha^n$ after n steps. We conclude that EDAP is robust against level asymmetry.

4. Phonon-assisted dephasing

In the previous two sections we have described adiabatic passage schemes in the solid state, and have demonstrated the flexibility of semiconductor nanostructures in engineering wavefunction and level schemes. However, so far we have not been too specific about possible decoherence channels, which is justified provided that the carrier states of lowest energy are sufficiently long lived and the losses of the interconnecting states are sufficiently moderate. Indeed, both requirements are perfectly fulfilled for spin memory and charge gates, considering the nano to microsecond timescale of spin coherence and the picosecond timescale of gating [6,20]. Yet, there exists another solid-state specific decoherence channel that requires further investigation, which is known as *phonon-assisted dephasing* [53–55]. Any carrier excitation in a semiconductor, such as an exciton or a surplus carrier, provides a perturbation to the lattice and causes a slight deformation of the lattice ions. In the language of quantized lattice vibrations, this deformation is described as a phonon cloud dressing the carrier excitation. When the carrier excitation moves, such as in our STIRAP or EDAP proposals described above, this phonon cloud will follow. Quite generally, only phonons with frequency above a certain threshold will be able to follow while low-frequency phonons cannot, which results in a transfer of coherence from the electronic system to the phonon environment.

To be more specific, in the following we consider the celebrated independent Boson model [53,55,12,11], described by the Hamiltonian

$$H = \sum_i \epsilon_i |i\rangle\langle i| + \sum_\lambda \omega_\lambda b_\lambda^\dagger b_\lambda^\dagger + \sum_{i\lambda} g_\lambda \langle i|e^{i\boldsymbol{q}_\lambda \boldsymbol{r}}|i\rangle \left(b_\lambda^\dagger + b_\lambda^\dagger\right)|i\rangle\langle i|. \tag{6}$$

Here, i denotes the different carrier states under consideration, $b_\lambda^\dagger$ is the bosonic creation operator for the phonon mode λ with energy ω_λ and wavevector $\boldsymbol{q}_\lambda$, and g_λ is the usual phonon coupling constant [53]. We emphasize that the carrier-phonon interaction in (6) is assumed to be diagonal in the carrier states, i.e., it cannot account for relaxation. Yet, as discussed in length in Ref. [53] and shown below it is responsible for pure dephasing. For simplicity, in the following we will consider a two-level system, i.e., $i = 0, 1$, corresponding to the states in a double-dot molecule, where the electron is in either the left or right (lower or upper) dot. The dots are assumed to be of spherical shape, and the wavefunctions are approximated by Gaussians with standard deviation L (details of our model and the definition of time units ω_c^{-1} is given in Refs. [12,52]). We assume that the coupling between the two states is of the form

$$H_c(t) = \Omega(t)(|0\rangle\langle 1| + |1\rangle\langle 0|) \tag{7}$$

with $\Omega(t)$ a time-dependent, external control field, e.g., gate voltage or laser pulse, where in the latter case one should introduce the rotating-wave approximation in Eq. (7). Suppose that the electron is initially in the left dot and the tunnel coupling is turned off. Because of the phonon coupling of Eq. (6) the lattice becomes distorted, as shown in Fig. 6c. When the coupling is turned on at time zero, the electron starts to tunnel from the left to the right dot and backwards again, as clearly shown in Fig. 6a. However, since the phonon cloud cannot follow the electron instantaneously, part of the quantum coherence is transferred from the electron system to the phonons, resulting in a coherence loss of the electron motion as evidenced by the damping of the oscillations shown in panel a. Such phonon-assisted decoherence has recently attracted great interest in both optics [52,54–57] and transport [40,58–60].

In fact, such decoherence can spoil the performance of quantum gates. Fig. 7a shows the result of time simulations for a quantum gate where the control field (shaded region) has a Gaussian shape and an area of π, i.e., in absence of phonon decoherence it would simply bring the electron from the left to the right dot. However, because of the phonon coupling described above the electronic system becomes entangled with the phonons, hereby suffering decoherence as evidenced by the finite left-dot population in Fig. 7a after completion of the gate. Noteworthy, this is a decoherence channel that affects the long-lived ground states and thus cannot be suppressed by STIRAP-type control strategies.

It should, however, be noted that, contrary to other decoherence channels in solids where the system's wavefunction acquires an uncontrollable phase through environment

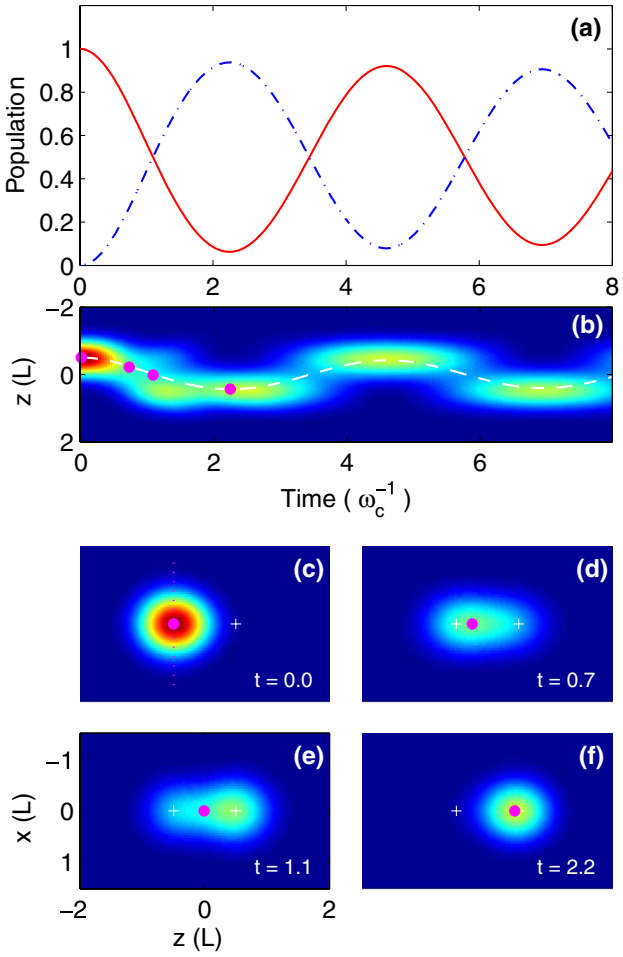

Fig. 6. Electron oscillations in a tunnel-coupled quantum-dot molecule in presence of phonon-assisted dephasing. Panel (a) shows the population in the left (solid line) and right (dashed-dotted line) dot. The electron wavepacket tunnels back and forth, and becomes damped because of phonon couplings. Panels (c–f) show snapshots of the lattice distortion, i.e., the Fourier transform of $Re(\langle b_\lambda \rangle)$, at four selected times. The crosses indicate the center of the two dots. Panel (b) shows the integrated lattice distortion (along x, cf. dotted line in panel a) and the mean position of the electron wavefunction (dashed line) as a function of time. For definition of units see Ref. [52]. We choose zero temperature throughout.

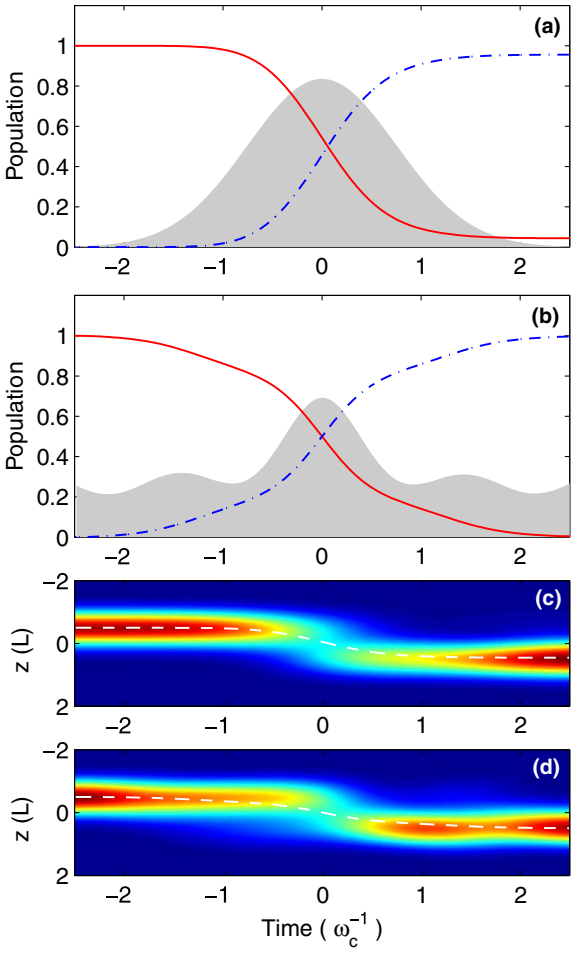

Fig. 7. Time simulation of a quantum gate. The time dependence of the control field is given by the shaded regions in panels a and b, and the population in the left and right dot by the solid and dashed-dotted line, respectively. Panel a shows the simulation for a Gaussian, and panel b for an optimized control field. For discussion, see text. Panels c and d show the time evolution of the integrated lattice distortion, as described in Fig. 6(caption).

coupling, in the independent Boson model the loss of phase coherence is due to the coupling of the electronic system to an ensemble of harmonic oscillators which all evolve with a coherent time evolution but different phase. This results, as shown above, in destructive interference and dephasing. On the other hand, the coherent nature of the state-vector evolution suggests that more refined control strategies might allow to suppress dephasing losses. A particularly flexible tool for the search of suitable control fields is provided by *optimal-control theory* [61,62], which has widespread applications in engineering, economy, and medical sciences, but has received only little attention in the field of solid-state control [63,52,64]. We shall now pose the question how the control field should be chosen in order to optimize the performance of the gate. Let T be the time when the gate is finished, and J the objective of the control, i.e., a function that rates the success of a given control. In the following we set J to the left-dot population at time T and search for the control field $\Omega(t)$ that minimizes J, i.e., we are seeking for solutions that minimize decoherence losses during gating. Optimal control theory accomplishes the search for improved control fields by converting the constrained minimization to an unconstrained one, by means of Lagrange multipliers, and formulating a numerical algorithm which, starting from an initial guess for $\Omega(t)$, succeedingly improves the control. Details of our numerical approach can be found in Refs. [63,52,12]. In panel b of Fig. 7 we show results for such an optimization of the control field: indeed, a control can be found (shaded region) which brings the electron from the left to the right dot without suffering significant decoherence losses. A similar finding was reported in Ref. [52] for the optical control of an exciton in a quantum dot. We attribute our finding to the fact that in the process of decoherence it takes some time for the system to become entangled with its environment. If during this entanglement buildup the system is acted upon by an appropriately designed control, it

becomes possible to channel back quantum coherence from the environment to the system. Our results thus reinforce quantum dots as viable candidates for quantum-information processing devices, and suggest that more refined control strategies might play an important role in the suppression of decoherence in future solid-state based quantum information devices.

Acknowledgements

U.H. and F.T. are indebted to Giovanna Panzarini for introducing us to the STIRAP scheme, which by that time was pure (quantum) mystery to us, and for initiating our first work in this field of research. Her memory will stay alive in our hearts. We are grateful to Elisa Molinari for most helpful discussions and generous support. This work has been supported in part by the Austrian science fund FWF. J.F. acknowledges support of the US ONR.

Appendix A. EDAP Hamiltonian

In this appendix we discuss in more detail the Hubbard Hamiltonian (3) within the subspace of the singlet, and double occupancy states. We use the following notation for triplet T (further indexed by spin projection S_z) and singlet S states on dots i and j (assuming $i<j$), as well as for double occupancy states D,

$$\begin{aligned}
&|T_1\rangle_{ij} = a_{i\uparrow}^+ a_{j\uparrow}^+|0\rangle, |T_{-1}\rangle_{ij} = a_{i\downarrow}^+ a_{j\downarrow}^+|0\rangle,\\
&|T_0\rangle_{ij} = (1/\sqrt{2})(a_{i\uparrow}^+ a_{j\downarrow}^+ - a_{j\uparrow}^+ a_{i\downarrow}^+)|0\rangle,\\
&|S\rangle_{ij} = (1/\sqrt{2})(a_{i\uparrow}^+ a_{j\downarrow}^+ + a_{j\uparrow}^+ a_{i\downarrow}^+)|0\rangle,\\
&|D\rangle_i = a_{i\uparrow}^+ a_{i\downarrow}^+|0.
\end{aligned} \tag{A.1}$$

Only States $|T_0\rangle$ and $|S\rangle$ are spin entangled. The Hilbert state, comprising 15 states, reduces to three three-dimensional triplet spaces which differ by S_z, and to one six-dimensional space of singlets. In the triplet space of $|T_{S_z}\rangle_{12}, |T_{S_z}\rangle_{13}$, and $|T_{S_z}\rangle_{23}$, the Hamiltonian is

$$H_{\text{triplet}} = \begin{pmatrix} \Delta & \sqrt{2}t_2 & 0 \\ \sqrt{2}t_2 & 0 & \sqrt{2}t_1 \\ 0 & \sqrt{2}t_1 & \Delta \end{pmatrix}, \tag{A.2}$$

while in the singlet space, spanned by the states $|D\rangle_1$, $|S\rangle_{12}$, $|S\rangle_{13}$, $|D\rangle_2$, $|S\rangle_{23}$, and $|D\rangle_3$, it is

$$H_{\text{singlet}} = \begin{pmatrix} U & \sqrt{2}t_1 & 0 & 0 & 0 & 0 \\ \sqrt{2}t_1 & \Delta & \sqrt{2}t_2 & \sqrt{2}t_1 & 0 & 0 \\ 0 & \sqrt{2}t_2 & 0 & 0 & \sqrt{2}t_1 & 0 \\ 0 & \sqrt{2}t_1 & 0 & U+2\Delta & \sqrt{2}t_2 & 0 \\ 0 & 0 & \sqrt{2}t_1 & \sqrt{2}t_2 & \Delta & \sqrt{2}t_2 \\ 0 & 0 & 0 & 0 & \sqrt{2}t_2 & U \end{pmatrix}. \tag{A.3}$$

The diagonalization of these Hamiltonians then gives the four trapped states of Eq. (4).

References

[1] M.A. Nielsen, I.L. Chuang, Quantum Computation and Quantum Information, Cambridge University Press, Cabmridge, 2000.
[2] H.A. Rabitz, M.M. Hsieh, C.M. Rosenthal, Science 303 (2004) 1998.
[3] K. Bergmann, H. Theuer, B.W. Shore, Rev. Mod. Phys. 70 (1998) 1003.
[4] N.Y. Vitanov, T. Halfmann, B.W. Shore, K. Bergmann, Annu. Rev. Phys. Chem. 52 (2001) 763.
[5] Z. Kis, F. Renzoni, Phys. Rev. A 65 (2002) 032318.
[6] F. Troiani, E. Molinari, U. Hohenester, Phys. Rev. Lett. 90 (2003) 206802.
[7] D. Bimberg, M. Grundmann, N. Ledentsov, Quantum Dot Heterostructures, Wiley, New York, 1998.
[8] F. Rossi (Ed.), Semiconductor Macroatoms, Imperial College Press, London, 2005.
[9] S. Reimann, M. Manninen, Rev. Mod. Phys. 74 (2002) 1283.
[10] W.G. van der Wiel, S. De Franceschi, J.M. Elzerman, T. Fujisawa, S. Tarucha, L.P. Kouwenhoven, Rev. Mod. Phys. 75 (2003) 1.
[11] T. Brandes, Phys. Rep. 408 (2005) 315.
[12] U. Hohenester, in: M. Rieth, W. Schommers (Eds.), Handbook of Theoretical and Computational Nanotechnology, American Scientific Publishers, Stevenson Ranch, CA, 2006.
[13] N.H. Bonadeo, J. Erland, D. Gammon, D. Park, D.S. Katzer, D.G. Steel, Science 282 (1998) 1473.
[14] X. Li, Y. Wu, D. Steel, D. Gammon, T.H. Stievater, D.S. Katzer, D. Park, C. Piermarocchi, L.J. Sham, Science 301 (2003) 809.
[15] J.R. Petta, J. Johnson, J.M. Taylor, E.A. Laird, A. Yacoby, M.D. Lukin, C.M. Marcus, M.P. Hanson, A.C. Gossard, Science 309 (2005) 2180.
[16] H. Kamada, H. Gotoh, J. Temmyo, Phys. Rev. Lett. 87 (2001) 246401.
[17] T.H. Stievater, X. Li, D.G. Steel, D. Gammon, D.S. Katzer, D. Park, C. Piermarocchi, L.J. Sham, Phys. Rev. Lett. 87 (2001) 133603.
[18] A. Zrenner, E. Beham, S. Stufler, F. Findeis, M. Bichler, B. Abstreiter, Nature 418 (2002) 612.
[19] U. Hohenester, F. Troiani, E. Molinari, G. Panzarini, C. Macchiavello, Appl. Phys. Lett. 77 (2000) 1864.
[20] J. Fabian, U. Hohenester, Phys. Rev. B 72 (2005) 201304(R).
[21] M. Bayer, P. Hawrylak, K. Hinzer, S. Fafard, M. Korkusinski, R. Wasilewski, O. Stern, A. Forchel, Science 291 (2001) 451.
[22] M. Rontani, F. Troiani, U. Hohenester, E. Molinari, Solid State Commun. 119 (2001) 309.
[23] F. Troiani, U. Hohenester, E. Molinari, Phys. Rev. B 65 (2002) 161301(R).
[24] A. Bertoni, M. Rontani, G. Goldoni, F. Troiani, E. Molinari, Appl. Phys. Lett. 85 (2004) 4729.
[25] E. Pazy, I. D'Amico, P. Zanardi, F. Rossi, Phys. Rev. B 64 (2001) 195320.
[26] Z. Kis, E. Paspalakis, J. Appl. Phys 96 (2004) 3435.
[27] R.G. Unanyan, N.V. Vitanov, K. Bergmann, Phys. Rev. Lett. 87 (2001) 137902.
[28] I. Žutić, J. Fabian, S. Das Sarma, Rev. Mod. Phys 76 (2004) 323.
[29] E. Pazy, E. Biolatti, T. Calarco, I. D'Amico, P. Zanardi, F. Rossi, P. Zoller, Europhys. Lett. 62 (2003) 175.
[30] B.W. Lovett, J.H. Reina, A. Nazir, G.A.D. Briggs, Phys. Rev. B 68 (2003) 205319.
[31] A. Imamoğlu et al., Phys. Rev. Lett. 83 (1999) 4204.
[32] A.S. Lenihan, M.V. Gurudev Dutt, D.G. Steel, S. Ghosh, P.K. Bhattacharya, Phys. Rev. Lett. 88 (2002) 223601.
[33] M. Paillard, X. Marie, P. Renucci, T. Amand, A. Jbeli, J.M. Gérard, Phys. Rev. Lett. 86 (2001) 1634.
[34] A. Imamoğlu, E. Knill, L. Tian, P. Zoller, Phys. Rev. Lett. 91 (2003) 017402.

[35] C. Santori, D. Fattal, J. Vukotic, G.C. Solomon, Y. Yamamoto, Nature (London) 419 (2002) 594.
[36] See: F. Troiani, J.I. Perea, C. Tejedor, cond-mat/0508578, and references therein.
[37] A. Kiraz, M. Atatüre, A. Imamoğlu, Phys. Rev. A 69 (2004) 32305.
[38] S. Bandyopadhyay, V.P. Roychowdhury, Superlatt. Microstruct. 22 (1997) 411.
[39] D. Loss, D.P. DiVincenzo, Phys. Rev. A 57 (1998) 120.
[40] T. Hayashi, T. Fujisawa, H.D. Cheong, Y.H. Jeong, Y. Hirayama, Phys. Rev. Lett. 91 (2003) 226804.
[41] J.R. Petta, A.C. Johnson, C.M. Marcus, M.P. Hanson, A.C. Gossard, Phys. Rev. Lett. 93 (2004) 186802.
[42] R. Hanson, B. Witkamp, L. Vandersypen, L.H. Willems van Beveren, J.M. Elzerman, L.P. Kouwenhoven, Phys. Rev. Lett. 91 (2003) 196802.
[43] G. Burkard, D. Loss, D.P. DiVincenzo, Phys. Rev. B 59 (1999) 2070.
[44] X. Hu, S. Das Sarma, Phys. Rev. A 61 (2000) 062301.
[45] R. Ruskov, A.N. Korotkov, Phys. Rev. B 67 (2003) 241305(R).
[46] J.M. Taylor, W. Dür, P. Zoller, A. Yacoby, C.M. Marcus, M.D. Lukin, Phys. Rev. Lett. 94 (2005) 236803.
[47] M. Blaauboer, D.P. DiVincenco, Phys. Rev. Lett. 95 (2005) 160402.
[48] P. Kral, J. Fiurasek, M. Shapiro, Phys. Rev. A 64 (2001) 023414.
[49] D. Loss, E.V. Sukhorukov, Phys. Rev. Lett. 84 (2000) 1035.
[50] X. Hu, S. Das Sarma, Phys. Rev. B 69 (2004) 115312.
[51] A.D. Greentree, J.H. Cole, A.R. Hamilton, L. Hollenberg, Phys. Rev. B 70 (2004) 235317.
[52] U. Hohenester, G. Stadler, Phys. Rev. Lett. 92 (2004) 196801.
[53] G.D. Mahan, Many-Particle Physics, Plenum Press, New York, 1981.
[54] P. Borri, W. Langbein, S. Schneider, U. Woggon, R.L. Sellin, D. Ouyang, D. Bimberg, Phys. Rev. Lett. 87 (2001) 157401.
[55] B. Krummheuer, V.M. Axt, T. Kuhn, Phys. Rev. B 65 (2002) 195313.
[56] A. Vagov, V.M. Axt, T. Kuhn, Phys. Rev. B 66 (2002) 165312.
[57] J. Förstner, C. Weber, J. Dankwerts, A. Knorr, Phys. Rev. Lett. 91 (2003) 127401.
[58] L. Fedichkin, A. Fedorov, IEEE Trans. Nanotechnol. 4 (2005) 65.
[59] S. Vorojtsov, E.R. Mucciolo, H.U. Baranger, Phys. Rev. B 71 (2005) 205322.
[60] V.N. Stavrou, X. Hu, Phys. Rev. B 72 (2005) 075362.
[61] A.P. Peirce, M.A. Dahleh, H. Rabitz, Phys. Rev. A 37 (1988) 4950.
[62] H. Rabitz, R. de Vivie-Riedle, M. Motzkus, K. Kompka, Science 288 (2000) 824.
[63] A. Borzì, G. Stadler, U. Hohenester, Phys. Rev. A 66 (2002) 053811.
[64] H. Jirari, W. Pötz, Phys. Rev. A 72 (2005) 013409.